Chinese Journal of Electronics
vol. 33, no. 4, pp. 1093–1103, July 2024
https://doi.org/10.23919/cje.2023.00.089

RESEARCH ARTICLE

Joint Communication-Caching-Computing Resource Allocation for Bidirectional Data Computation in IRS-Assisted Hybrid UAV-Terrestrial Network

Yangzhe LIAO, Lin LIU, Yuanyan SONG, and Ning XU

School of Information Engineering, Wuhan University of Technology, Wuhan 430070, China

Corresponding author: Ning XU, Email: xuning@whut.edu.cn
Manuscript Received March 23, 2023; Accepted June 16, 2023

Abstract — Joint communication-caching-computing resource allocation in wireless inland waterway communications enables resource-constrained unmanned surface vehicles (USVs) to provision computation-intensive and latency-sensitive tasks forward beyond fifth-generation (B5G) and sixth-generation (6G) era. The power of such resource allocation cannot be fully studied unless bidirectional data computation is properly managed. A novel intelligent reflecting surface (IRS)-assisted hybrid UAV-terrestrial network architecture is proposed with bidirectional tasks. The sum of uplink and downlink bandwidth minimization problem is formulated by jointly considering link quality, task execution mode selection, UAVs trajectory, and task execution latency constraints. A heuristic algorithm is proposed to solve the formulated challenging problem. We divide the original challenging problem into two subproblems, i.e., the joint optimization problem of USVs offloading decision, caching decision and task execution mode selection, and the joint optimization problem of UAVs trajectory and IRS phase shift-vector design. The Karush–Kuhn–Tucker conditions are utilized to solve the first subproblem and the enhanced differential evolution algorithm is proposed to solve the latter one. The results show that the proposed solution can significantly decrease bandwidth consumption in comparison with the selected advanced algorithms. The results also prove that the sum of bandwidth can be remarkably decreased by implementing a higher number of IRS elements.
Keywords — Intelligent reflecting surface, Unmanned surface vehicles, Bidirectional data computation, Resource allocation.
Citation — Yangzhe LIAO, Lin LIU, Yuanyan SONG, *et al.*, "Joint Communication-Caching-Computing Resource Allocation for Bidirectional Data Computation in IRS-Assisted Hybrid UAV-Terrestrial Network," *Chinese Journal of Electronics*, vol. 33, no. 4, pp. 1093–1103, 2024. doi: 10.23919/cje.2023.00.089.

I. Introduction

In the fifth-generation (5G) era, wireless communication networks performance enhancement either focuses on the mobile user side or the mobile network operator (MNO) [1],[2]. From MNOs' perspective, one commonly used method to satisfy the ever-increasing quality of service (QoS) requirements of mobile users is to deploy more multiple-antenna terrestrial base stations (TBSs) [3]. However, in the current paradigm of wireless communication networks, the significantly expanding data traffic, emerging big data services, and ubiquitous deployments of mobile devices have brought significant technical challenges, motivating academia and industry to move forward beyond 5G (B5G) and sixth-generation (6G). With the popularity of unmanned surface vehicles (USVs), one of the promising technologies in B5G and 6G, namely wireless inland waterway communication, has attracted considerable attention. In particular, USVs are equipped with communication and computation capabilities and typically integrated with a list of onboard sensors, such as global positioning systems, radar, sonars, altitude and water-depth detectors, and so forth. Although MNOs have made significant efforts regarding enhancing the communication quality between USVs and TBSs, there are still numerous technical disadvantages that are chal-

Associate Editor: Prof. Hai-Tao ZHAO, Nanjing University of Posts and Telecommunications.

lenging to be solved to fulfil fully functioning inland waterway communications. First, USVs are generally capable of measuring line-of-sight (LoS) range and relative bearing angle, struggling to satisfy the strict ship-shore transmission link quality. The currently used technologies, such as very high frequency and ultra-high frequency communications, have been proven that can only support data rates up to 9.6 kbit/s, which may result in significant transmission delay and even packet loss [4]. In addition, MNOs suffer significant profit reductions to deploy 5G telecommunication infrastructure such as TBSs and offer global Internet connectivity through low earth orbit satellites. Although satellites can play as intermediate nodes directly communicating with USVs to offer real-time connectivity, the expenditure of satellite-based communications is high and cannot be widely utilized to serve budget-limited USVs [5].

Owing to the fast-growing progress of intelligent reflecting surface (IRS), academia and industry have enthusiastically envisioned and scheduled the B5G and 6G wireless communication networks to fulfill the strict QoS of wireless inland waterway communications [6], [7]. In particular, IRS is a two-dimensional artificial electromagnetic surface, composed of a large array of passive reflecting elements, which can flexibly adjust electromagnetic functionalities, such as wavefront shaping, signal reflection, and frequency shifting of the incident signals via a software-defined manner. In this way, IRS is capable of reconfiguring wireless propagation environments without deploying additional telecommunication infrastructures and consuming almost zero energy. By deploying the smart radio environment into the current network, the wireless channels can be programmed to provision network performance with a higher channel capacity for wireless inland waterway communications. In [8], the authors reported that IRS-assisted wireless networks are envisioned to revolutionize the current network paradigm and are expected to play an active role, especially in offering better quality links for the network edge users. In [9], the authors mentioned that IRS-assisted communications provide better signal strength and mitigate interference between the transmitter and receiver in comparison with relaying and backscatter communications. The authors in [10] proposed numerous typical IRS-assisted transmission models, where IRS can be coated on walls, building surfaces, or carried by aerial platforms. The results show that an IRS-assisted transmission scheme can transform traditional radio environments into smart environments and enhance communication, caching and computing performance.

The integration between IRS and UAVs paves the way for developing B5G and 6G wireless networks to offer ubiquitous communication services [11]–[13]. In particular, UAV communications have emerged as promising technologies to satisfy computation intensive or latency sensitive tasks by utilizing as relays, base stations (BSs), or flying mobile edge computing (MEC) servers. The authors in [14] reported that owing to outstanding characteristics of UAVs, such as easy deployment and adaptive altitude, UAVs have gained considerable attention in creating LoS links with ground mobile users lacking ground telecommunication infrastructure. The authors in [15] proposed that an IRS can offer LoS transmission links to mobile users by intelligently adjusting its reflection coefficients rather than deploying multiple antennas on UAVs. The authors in [7] formulated a network energy minimization problem by jointly considering UAV trajectory and IRS phase shift vector design. The results show that the novel IRS-assisted UAV data transmission scheme can considerably improve network performance, such as coverage, energy efficiency, and so forth. The authors in [16] mounted IRS onto a UAV to enhance the achievable data rate for ground mobile users under weak link quality scenarios. In particular, the passive beamforming controlled by IRS can reflect the dissipated signals transmitted from UAVs to ground mobile users. The authors in [17] proposed an IRS-assisted UAV communication network architecture, where IRS is coated on the building to improve signal transmission quality from UAV to ground mobile devices. The authors in [18] implemented aerial IRS by integrating IRS with balloons or UAVs to realize full reflection and create air-to-ground LoS channels. The authors in [19] deployed IRS in an MEC system, where the computation tasks at resource-limited mobile devices can be offloaded to resource-rich MEC servers. The authors in [20] proposed the energy minimization optimization problem by jointly designing user scheduling, UAV trajectory, and IRS reflection coefficient. The results show that the network energy consumption can be considerably decreased compared with that without utilizing IRS or designing the UAV trajectory. Although significant efforts have been made regarding the cooperative design for USV-UAV systems, the research on the joint utilization of UAV and IRS in air-ground networks is still at the early stage, especially in wireless inland waterway environments.

With the ever-expanding intensive communication and computation requirements of USVs, the concept of bidirectional computation task has emerged as an important perspective use case in B5G and 6G era, originally derived from immersive extended reality with multimodal data, where they render the live scene by jointly computing user features, 3D positions and video data downloaded from the Internet [20]. Moreover, with the ever-growing intensive communication and computation requirements of USVs, bidirectional mission offloading has emerged as an effective perspective solution for transferring the majority of energy consumption from USVs to UAVs, which also provides data communication links for USVs consuming additional bandwidth resource. The authors in [21] formulated the mobile devices execution latency minimization problem considering a novel bidirectional task model. However, this research assumed input data generated by mobile devices and ignored input data generated by the Internet. The authors in [22] proposed a novel MEC network architecture with multimodal semantic communication. The results show that the proposed bidirectional computation task model is more realistic for emerging AI-enabled applications, where a portion of data is generated from mobile users and the rest is derived from the Internet. The authors in [23] proposed a bidirectional task model and formulated the network bandwidth minimization problem by jointly considering computation and caching resource allocation. However, this work ignored the performance enhancement from mobile users' perspective, which may lead to unsatisfactory user-perceived quality of experience. The authors in [24] proposed the bidirectional computation task model, where each bidirectional task can be executed via three ways, i.e., local computing with local caching, local computing without local caching, and MEC computing. Note that although the joint communication, caching and computation resource allocation for the bidirectional computation task execution can enhance bandwidth efficiency, the research regarding IRS-assisted hybrid UAV-terrestrial network bandwidth consumption has not been fully addressed yet.

In this paper, a novel IRS-assisted hybrid UAV-terrestrial network architecture of wireless inland waterway communications to handle bidirectional data computation is proposed. This paper formulated the sum of uplink and downlink bandwidth minimization problem by jointly considering link quality, task execution mode selection, UAV trajectory and task execution latency constraints. To solve the formulated challenging problem, we first divide the original problem into two subproblems. Then, a heuristic solution is proposed, where the joint optimization problem of USVs offloading decision, caching decision, and task execution mode selection is solved by using the Karush–Kuhn–Tucker (KKT) conditions; the joint optimization problem of UAVs trajectory and IRS phase shift-vector design is solved by utilizing the enhanced differential evolution (DE) algorithm. The results show that the proposed solution can significantly reduce the sum of uplink and downlink bandwidth consumption in comparison with the two selected advanced algorithms. Also, the results demonstrate that the sum of uplink and downlink bandwidth consumption can be significantly decreased by implementing a higher number of IRS elements.

The remainder of this paper is organized as follows. Section II introduces the proposed IRS-assisted hybrid UAV-terrestrial network architecture and the formulated network bandwidth minimization problem. Section III presents the proposed heuristic solution in detail. Section IV summarizes the key performance parameters of the proposed solution and compares it with two selected advanced algorithms. Section V concludes the paper.

II. System Model and Problem Formulation

The proposed novel IRS-assisted hybrid UAV-terrestrial network architecture for wireless inland waterway communications considering joint communication, caching, and computing for bidirectional data computation is shown in Figure 1. In this system, tethered UAVs are deployed and dynamically form virtual clusters with TBSs to serve USVs, and each tethered UAV $l \in \mathcal{L}$ is connected with an MEC server via cable and equipped with K passive reflecting elementa IRS[*1]. Moreover, a set of S marine SATs denoted by $\mathcal{S}$ are deployed to offer temporary wireless communication services for USVs, such as path planning, automatic navigation, and so forth. Each UAV is assumed to fly at the fixed height H and cannot serve more than one USV simultaneously. Note that the coordinates of UAVs are determined once virtual clusters are formed.

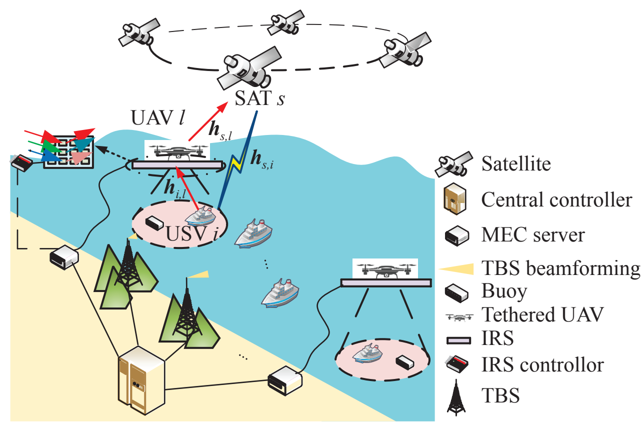

Figure 1 The proposed IRS-assisted hybrid UAV-terrestrial network architecture.

In this paper, the 3D Cartesian coordinate is considered. Considering each virtual cluster, the coordinates of edge server, UAV l, and its corresponding hovering coordinate are denoted by $\boldsymbol{q}_0$, $\boldsymbol{q}_l$, and $\boldsymbol{s}_l$, respectively. Each bidirectional task generated by USV i during each equal-length time slot can be characterized by $U_i \triangleq (D_i^l, D_i^s, O_i, F_i, \tau_i)$, where D_i^l and D_i^s are task data size (in bits) generated by USV i and remote input data designated from SAT s, respectively. O_i is the size of output data. F_i and τ_i indicate the number of required CPU cycles and the maximum allowable time to execute U_i, respectively. Note that each edge server is connected with one L-antenna TBS via optic fiber and thus the transmission latency between them can be ignored.

1. IRS-assisted channel models

The phase shift-vector of each IRS l is denoted by $\boldsymbol{\theta}_l = [\theta_{l,1}, \theta_{l,2}, \ldots, \theta_{l,k}, \ldots, \theta_{l,K}]^{\mathrm{T}}$, where $\theta_{l,k} \in [0, 2\pi), k \in \{1, 2, \ldots, K\}$. In accordance with [21], we assume that each IRS l follows full reflection. The corresponding re-

[*1] For simplification purposes, since each UAV is integrated with IRS, IRS l refers to IRS integrated by UAV l.

flection coefficient matrix can be expressed as

$$\boldsymbol{\Theta}=\begin{bmatrix} e^{j\theta_{l,1}} & 0 & \cdots & 0 \\ 0 & e^{j\theta_{l,2}} & \cdots & 0 \\ \vdots & \vdots & \ddots & \vdots \\ 0 & 0 & \cdots & e^{j\theta_{l,K}} \end{bmatrix},\ l\in\mathcal{L} \tag{1}$$

The equivalent baseband channels from SAT s to USV i, SAT s to UAV l, and UAV l to USV i can be denoted by $\boldsymbol{h}_{s,i}\in\mathbb{R}^{M\times 1}$, $\boldsymbol{h}_{s,l}\in\mathbb{R}^{M\times K}$, and $\boldsymbol{h}_{i,l}\in\mathbb{R}^{K\times 1}$, $s\in\mathcal{S}, i\in\mathcal{I}, l\in\mathcal{L}$, respectively. Denote H_s and R_s as the height and the distance between the center of SAT s coverage area and its central beam, respectively. Denote that $\tilde{h}$ characterizes the small-scale fading of SAT-USV link, which can be expressed as

$$\tilde{h}=A\exp(j\psi)+Z\exp(j\phi) \tag{2}$$

where $\psi\in[0,\pi]$ is the stationary random phase and A denotes the amplitude, which obeys Rayleigh distribution. The amplitude Z follows Nakagami-m distribution and $\phi\in[0,\pi]$ is the deterministic phase. Let λ be the carrier wavelength. The channel gain between SAT s and USV i can be expressed as

$$\boldsymbol{h}_{s,i}=\sqrt{b(\boldsymbol{\varphi}_{s,i})}\tilde{h}\lambda\Big/(4\pi\sqrt{H_s^2+R_s^2}),\ s\in\mathcal{S}, i\in\mathcal{I} \tag{3}$$

where $b(\boldsymbol{\varphi}_{s,i})$ is beam gain factor of SAT s-UAV i link, which can be given as

$$b(\boldsymbol{\varphi}_{s,i})=b_{\max}\left(\frac{J_1(u_{s,i})}{2u_{s,i}}+36\frac{J_3(u_{s,i})}{u_{s,i}^3}\right)^2,\ s\in\mathcal{S}, i\in\mathcal{I} \tag{4}$$

where $b_{\max}$ is the maximum achievable satellite-USV link beam gain and $\varphi_{3\text{dB}}$ denotes the 3 dB angle. $\boldsymbol{\varphi}_{s,i}=[\varphi_{s,i}^1, \varphi_{s,i}^2,\dots,\varphi_{s,i}^M]^{\mathrm{T}}$ is the angle between the beam center of SAT s and USV i. $J_1(\cdot)$ and $J_3(\cdot)$ represent order one and order three of the first-kind Bessel functions, respectively. $u_{s,i}=2.07123\sin\varphi_{s,i}/\sin\varphi_{3\text{dB}}$. In this way, the channel gain between SAT s and UAV l can be expressed as

$$\boldsymbol{h}_{s,l}=\sqrt{b\left(\boldsymbol{\varphi}_{s,l}\right)}\tilde{h}\lambda\Big/(4\pi\sqrt{H_s^2+d_s^2}),\ s\in\mathcal{S}, l\in\mathcal{L} \tag{5}$$

where $\boldsymbol{\varphi}_{s,l}=[\varphi_{s,l}^1,\varphi_{s,l}^2,\dots,\varphi_{s,l}^M]^{\mathrm{T}}$ denotes the angle between UAV l and beam center of SAT s. The channel gain between UAV l and USV i via IRS-assisted data transmission can be given as

$$\begin{aligned}\boldsymbol{h}_{i,l}=&\sqrt{d_{i,l}^{-\beta}}\left[1,e^{-j\frac{2\pi d}{\lambda}\zeta_{i,l}},\dots,e^{-j\frac{2(K-1)\pi d}{\lambda}\zeta_{i,l}}\right]^{\mathrm{T}},\\ &i\in\mathcal{I}, l\in\mathcal{L}\end{aligned} \tag{6}$$

where $d_{i,l}$ denotes the transmission distance between UAV l and USV i. β and $\zeta_{i,l}$ indicate the link path loss (PL) coefficient and the cosine of the angle of arrival of the incident signal from IRS l to USV i, respectively. d is the separation distance between any two successive IRS elements.

2. Caching, communication and computing models

Let the binary offloading decision variable of USV i be α_i, where $\alpha_i=1$ indicates USV i decides to offload data D_i^l and $\alpha_i=0$ otherwise. Moreover, denote the caching decision variable of USV i as c_i representing whether to cache remote input data D_i^s, where $c_i=1$ means the remote input data D_i^s is cached by USV i and $c_i=0$ otherwise. Define $x_{i,a}\in\{0,1\}, i\in\mathcal{I}, a\in\{1,2,3\}$, where $x_{i,a}=1$ means that task i is executed by a-th mode and $x_{i,a}=0$ otherwise. In this manner, each task can be executed via the following three execution modes.

Local execution with local caching mode: This execution mode only requires the downlink bandwidth. Each USV i computes D_i^l locally and caches remote data D_i^s from SAT s. In this way, one can obtain that $\alpha_i=0$, $c_i=0$, and $x_{i,1}=1$.

$$\mathcal{C}1:\sum_i D_i^s c_i\le C_i,\ i\in\mathcal{I} \tag{7}$$

Since task execution time cost cannot exceed the maximum time allowance, one has

$$\mathcal{C}2:\frac{(D_i^l+D_i^s)F_i}{f_i}(1-\alpha_i)c_i\le\tau_i,\ i\in\mathcal{I} \tag{8}$$

where f_i is the computation capability of USV i.

Local execution with remote caching mode: This execution mode only requires the downlink bandwidth. Each USV i computes D_i^l locally and caches remote data D_i^s from SAT s. In this way, one can obtain that $\alpha_i=0$, $c_i=0$, and $x_{i,2}=1$. Let B_i^D be the allocated downlink bandwidth to transmit output data O_i, one has

$$\mathcal{C}3:\frac{O_i}{\left(\tau_i-\dfrac{(D_i^l+D_i^s)F_i}{f_i}\right)\log\left(1+\dfrac{p_s h^2}{N_0}\right)}\le B_i^D,\ i\in\mathcal{I} \tag{9}$$

where p_s is the transmission power of SAT s, h is the channel coefficient, and N_0 is the average power spectral density of noise.

IRS-assisted MEC mode: This execution mode requires uplink and downlink bandwidth. Considering each USV i in the first stage, D_i^l and D_i^s are transmitted to edge server by USV i and SAT s, respectively. Then, O_i is transmitted to USV i after executed by edge server. In this way, one can obtain that $\alpha_i=1$, $c_i=0$, and $x_{i,3}=1$. The signal received by SAT s from USV i via IRS-assisted offloading method can be given as

$$y_i=\boldsymbol{w}_{s,i}^{\mathrm{H}}\sqrt{p_i^{\mathrm{tr}}}(\boldsymbol{h}_{s,i}+\boldsymbol{h}_{s,l}\boldsymbol{\Theta}\boldsymbol{h}_{i,l})s_i+n,\ s\in\mathcal{S}, i\in\mathcal{I}, l\in\mathcal{L} \tag{10}$$

where s_i is the transmitted data symbol with average unity power, i.e., $\mathbb{E}(|s_i|^2)=1$. $\boldsymbol{w}_{s,i}\in\mathbb{R}^{M\times 1}$ represents the beamforming vector of SAT s, and n denotes the noise. The corresponding signal to interference plus noise ratio (SINR) between USV i and SAT s, denoted by $\gamma_{b,i}(\boldsymbol{\theta},\boldsymbol{q})$, which can be expressed as

$$\gamma_{s,i}(\boldsymbol{\theta},\boldsymbol{q}) = \frac{p_i^{\mathrm{tr}}\|\boldsymbol{w}_{s,i}^{\mathrm{H}}(\boldsymbol{h}_{s,i}+\boldsymbol{h}_{s,l}\boldsymbol{\Theta}\boldsymbol{h}_{i,l})\|^2}{\sum_{m=1,m\neq i}^{I} p_m^{\mathrm{tr}}\|\boldsymbol{w}_{s,i}^{\mathrm{H}}(\boldsymbol{h}_{s,m}+\boldsymbol{h}_{s,l}\boldsymbol{\Theta}\boldsymbol{h}_{i,l})\|^2+\sigma^2\|\boldsymbol{w}_{s,i}^{\mathrm{H}}\|^2}, \quad i,m\in\mathcal{I}, i\neq m, l\in\mathcal{L} \tag{11}$$

where p_i^{tr} and p_m^{tr} indicate the transmission power of USV i and m, respectively. The corresponding offloading time cost can be expressed as

$$t_i^o = \frac{\alpha_i D_i^l}{B_i^U \log(1+\gamma_{s,i}(\boldsymbol{\theta},\boldsymbol{q}))},\ i\in\mathcal{I} \tag{12}$$

where B_i^U is the allocated uplink bandwidth of USV i. The corresponding latency constraint should satisfy

$$\mathcal{C}4: \left(t_i^o + \frac{(D_i^l+D_i^s)F_i}{f} + \frac{O_i}{B_i^D\log\left(1+\dfrac{p_s h^2}{N_0}\right)}\right)\alpha_i \le \tau_i, \quad i\in\mathcal{I} \tag{13}$$

where f is the computation capability of MEC server.

3. UAV trajectory model

Denote the maximum flying speed of each UAV l by $v_l^{\max}$, one has

$$\mathcal{C}5: \|\boldsymbol{q}_l'\| \le v_l^{\max},\ l\in\mathcal{L} \tag{14}$$

To promise the channel link quality, the transmission distance between UAV l and USV i cannot exceed the maximum available communication distance $d_{i,l}^{\max}$, one has

$$\mathcal{C}6: d_{i,l} = \|\boldsymbol{q}_l - \boldsymbol{q}_i\| \le d_{i,l}^{\max},\ i\in\mathcal{I}, l\in\mathcal{L} \tag{15}$$

Let the maximum tether length of each UAV be $L_{\max}$. One has

$$\mathcal{C}7: \|\boldsymbol{q}_l-\boldsymbol{q}_0\|^2 + H^2 \le L_{\max}^2,\ l\in\mathcal{L} \tag{16}$$

4. Problem formulation

Denote $\gamma_{s,i}^{\mathrm{th}}$ as the predetermined acceptable SINR threshold between USV i and SAT s link. In this paper, we aim to minimize the sum of uplink and downlink bandwidth by jointly considering link quality, task execution mode selection, UAVs trajectory, and task execution latency constraints, which can be formulated as

$$\begin{aligned}
\mathcal{P}1: &\min_{\boldsymbol{q},\boldsymbol{\theta},\boldsymbol{a},\boldsymbol{c},\boldsymbol{x}} \sum_{t\in\mathcal{T}}\sum_{i\in\mathcal{I}}(B_i^U+B_i^D)\\
\text{s.t. } &\mathcal{C}1-\mathcal{C}7,\\
&\mathcal{C}8: \gamma_{s,i}\ge\gamma_{s,i}^{\mathrm{th}}, i\in\mathcal{I}, s\in\mathcal{S},\\
&\mathcal{C}9: \alpha_i\in\{0,1\}, i\in\mathcal{I},\\
&\mathcal{C}10: c_i\in\{0,1\}, i\in\mathcal{I},\\
&\mathcal{C}11: x_{i,a}\in\{0,1\}, i\in\mathcal{I}, a\in\{1,2,3\}
\end{aligned} \tag{17}$$

where $\mathcal{C}1$ indicates that the local cached data size of USV i cannot exceed the maximum caching capacity C_i. $\mathcal{C}2$ demonstrates that local task execution time cost should satisfy the latency constraint. $\mathcal{C}3$ and $\mathcal{C}4$ reveal the minimal required downlink bandwidth and the task execution latency constraint when USV i selects local execution with remote caching mode and IRS-assisted edge computing mode, respectively. $\mathcal{C}5$–$\mathcal{C}7$ demonstrates tethered UAVs trajectory constraints. $\mathcal{C}8$ illustrates that SINR of each USV i-SAT s link cannot be less than the predetermined threshold $\gamma_{s,i}^{\mathrm{th}}$. $\mathcal{C}9$–$\mathcal{C}11$ specify the offloading decision variable, caching variable, and execution mode selection variable of USV i are 0-1 binary variables, respectively.

Note that $\mathcal{P}1$ is a non-linear non-convex optimization problem and is extremely challenging to be solved. First, due to the existence of 0-1 binary variables, the widely utilized highly efficient algorithms, such as genetic algorithm, DE, and particle swarm optimization, cannot be directly utilized to solve $\mathcal{P}1$ [25]. Although a list of advanced non-convex optimization methods and AI algorithms, such as accelerated gradient method and reinforcement learning and so forth, have been expected to solve non-convex optimization efficiently, the computational complexity to solve $\mathcal{P}1$ becomes extremely complicated and may not be solved even suffering remarkably computation resource and time cost since the optimization variables $\boldsymbol{q}$ and $\boldsymbol{\theta}$ in $\mathcal{P}1$ are closely coupled. Inspired by DE algorithm, note that since not all UAVs participating in bidirectional data computation are able to serve USVs in this paper, encoding the coordinates of each UAV may bring the redundant search space and decrease the network performance. Moreover, due to the existence of optimization variable $\boldsymbol{\theta}$, it is extremely challenging to solve $\mathcal{P}1$ directly by using the traditional optimization methods. As a result, aiming to efficiently solve $\mathcal{P}1$, a heuristic solution can be proposed by jointly considering convergence speed and optimizing each phase shift-vector of IRS.

III. The Proposed Solution

1. The joint optimization of USVs offloading decision, caching decision, and task execution mode selection

Given any feasible $\boldsymbol{q}$ and $\boldsymbol{\theta}$, $\mathcal{P}1$ can be reduced as

$$\mathcal{P}1.1: \min_{\boldsymbol{\alpha},\boldsymbol{c},\boldsymbol{x}} \sum_{i\in\mathcal{I}} (B_i^U + B_i^D)$$
$$\text{s.t.} \quad \mathcal{C}9 - \mathcal{C}11 \tag{18}$$

In this paper, we focus on IRS-assisted edge computing mode, i.e., $\alpha_i = 0$, $c_i = 0$, and $x_{i,3} = 1$. One should note that the performance analysis of local execution with local caching mode and local execution with remote caching mode can be extended based on the solution obtained in this section. In this way, $\mathcal{P}1.1$ can be transformed into

$$\begin{aligned} \hat{\mathcal{P}}1.1: \quad & \min_{B_i^U, B_i^D} \sum_{i\in\mathcal{I}} (B_i^U + B_i^D) \\ \text{s.t.} \quad \widetilde{\mathcal{C}4}: \quad & \frac{D_i^l}{B_i^U \log(1+\gamma_{b,i}(\boldsymbol{\theta},\boldsymbol{q}))} + \frac{O_i}{B_i^D \log\left(1+\frac{p_s h^2}{N_0}\right)} \\ & \le \tau_i - \frac{(D_i^l + D_i^s)F_i}{f}, i\in\mathcal{I}, \\ & B_i^U > 0, i\in\mathcal{I}, \\ & B_i^D > 0, i\in\mathcal{I} \end{aligned} \tag{19}$$

Proposition 1 The optimal value to the objective function of $\hat{\mathcal{P}}1.1$ can be given as $B_i^{U*} + B_i^{D*} = \frac{\frac{D_i^l}{\log(1+\gamma_{b,i}(\boldsymbol{\theta},\boldsymbol{q}))} + \frac{O_i}{\log(1+\frac{p_s h^2}{N_0})} + 2\sqrt{\frac{D_i^l}{\log(1+\gamma_{b,i}(\boldsymbol{\theta},\boldsymbol{q}))}\frac{O_i}{\log(1+\frac{p_s h^2}{N_0})}}}{(\tau_i - \frac{(D_i^l+D_i^s)F_i}{f})}$.

Proof Let $A_1(\boldsymbol{\theta},\boldsymbol{q}) = \frac{D_i^l}{\log(1+\gamma_{b,i}(\boldsymbol{\theta},\boldsymbol{q}))}$, $A_2 = \frac{O_i}{\log(1+\frac{p_s h^2}{N_0})}$, and $A_3 = \tau_i - \frac{(D_i^l + D_i^s)F_i}{f}$, where A_1, A_2, and A_3 are constants. After introducing A_1, A_2, and A_3, $\hat{\mathcal{P}}1.1$ can be rewritten as

$$\begin{aligned} \widetilde{\mathcal{P}}1.1: \min_{B_i^U, B_i^D} & \sum_{t\in\mathcal{T}} \sum_{i\in\mathcal{I}} (B_i^U + B_i^D) \\ \text{s.t.} \quad & \frac{A_1}{B_i^U} + \frac{A_2}{B_i^D} \le A_3, \\ & B_i^U > 0, i\in\mathcal{I}, \\ & B_i^D > 0, i\in\mathcal{I} \end{aligned} \tag{20}$$

One can observe that $\widetilde{\mathcal{P}}1.1$ is a convex optimization problem and can be directly solved by utilizing KKT conditions [26]. As a result, the optimal solution can be given as

$$B_i^{U*} = \frac{A_1 + \sqrt{A_1 A_2}}{A_3} \tag{21}$$

$$B_i^{D*} = \frac{A_2 + \sqrt{A_1 A_2}}{A_3} \tag{22}$$

Note that $B_i^{U*} > 0$ and $B_i^{D*} > 0$. As such, the optimal value to the objective function of $\widetilde{\mathcal{P}}1.1$ can be given as $\frac{A_1(\boldsymbol{\theta},\boldsymbol{q}) + A_2 + 2\sqrt{A_1(\boldsymbol{\theta},\boldsymbol{q})A_2}}{A_3}$.

This completes the proof.

2. The joint optimization of UAVs trajectory and IRS phase shift-vector

According to Section III.1, given any feasible $\boldsymbol{\alpha}$, $\boldsymbol{c}$, and $\boldsymbol{x}$, $\mathcal{P}1$ can be reduced as

$$\mathcal{P}1.2: \min_{\boldsymbol{q},\boldsymbol{\theta}} \sum_{i\in\mathcal{I}} \frac{A_1(\boldsymbol{\theta},\boldsymbol{q}) + A_2 + 2\sqrt{A_1(\boldsymbol{\theta},\boldsymbol{q})A_2}}{A_3}$$
$$\text{s.t.} \quad \mathcal{C}5 - \mathcal{C}8 \tag{23}$$

Transform $\mathcal{P}1.2$ into the problem of minimizing the value of $A_1(\boldsymbol{\theta},\boldsymbol{q})$. In this way, $\mathcal{P}1.2$ can be rewritten as

$$\widetilde{\mathcal{P}}1.2: \min_{\boldsymbol{q},\boldsymbol{\theta}} \sum_{t\in\mathcal{T}} \sum_{i\in\mathcal{I}} \frac{D_i^l}{\log_2(1+\gamma_{b,i}(\boldsymbol{\theta},\boldsymbol{q}))}$$
$$\text{s.t.} \quad \mathcal{C}5 - \mathcal{C}8 \tag{24}$$

Note that $\widetilde{\mathcal{P}}1.2$ is still an non-deterministic polynomial hard problem and challenging to be solved. In this paper, the enhanced DE algorithm is proposed to solve $\widetilde{\mathcal{P}}1.2$. The main process of the proposed algorithm is introduced in detail.

Initialization Denote the current iteration, the maximum number of iterations, and the current coordinate of UAV l by g, $g_{\max}$, and $\boldsymbol{q}_l^g$, respectively. At the network initialization stage, the coordinates of UAV swarm at the g-th generation can be encoded into $\mathcal{Q}_t^g = \{\boldsymbol{q}_1^g, \dots, \boldsymbol{q}_l^g, \dots, \boldsymbol{q}_L^g\}, g \in \{1, 2, \dots, g_{\max}\}$, where $\boldsymbol{q}_l^g$ can be expressed as

$$\boldsymbol{q}_l^g = (q_{l,1}^g, q_{l,2}^g, \dots, q_{l,N}^g, \dots, q_{l,2N}^g),\ l\in\mathcal{L} \tag{25}$$

where N represents the length of encoding.

Mutation During the g-th generation, one can randomly select three individuals, e.g., $\boldsymbol{q}_{r1}^g$, $\boldsymbol{q}_{r2}^g$, and $\boldsymbol{q}_{r3}^g$, to generate mutation operator $\boldsymbol{v}_l^g$, which can be expressed as

$$\begin{aligned} & \boldsymbol{v}_l^g = \boldsymbol{q}_{r1}^g + F_0(\boldsymbol{q}_{r2}^g - \boldsymbol{q}_{r3}^g), \\ & l, r1, r2, r3 \in \mathcal{L},\ l \ne r1 \ne r2 \ne r3 \end{aligned} \tag{26}$$

where F_0 is the scaling factor.

Crossover To enhance the potential diversity of the population, $\boldsymbol{v}_l^g$ and $\boldsymbol{q}_l^g$ are utilized to generate the crossover operator denoted by $\boldsymbol{u}_l^g = (u_{l,1}^g, u_{l,2}^g, \dots, u_{l,l'}^g, \dots, u_{l,N}^g, \dots, u_{l,2N}^g), l\in\mathcal{L}$. In accordance with [27], the commonly used binomial crossover method is utilized, which can be formulated as

$$u_{l,l'}^g = \begin{cases} v_{l,l'}^g, & \text{if } \mathrm{rand}_{l'} \le \mathrm{CR} \text{ or } l' = l'_{\mathrm{rand}} \\ q_{l,l'}^g, & \text{otherwise} \end{cases} \tag{27}$$

where $\mathrm{rand}_{l'}$ denotes a uniformly distributed number ranging from [0, 1] for each l' and CR denotes the crossover control parameter. l'_{rand} is a randomly selected integer from $[1, 2N]$ to promise $\boldsymbol{u}_l^g$ is different from $\boldsymbol{q}_l^g$ in at least one dimension.

Fitness function design The corresponding phase shift-vector $\boldsymbol{\theta}_l$ of IRS l is considered to evaluate the fitness value of $\boldsymbol{u}_l^g$. Given any feasible $\boldsymbol{q}$, the problem $\widetilde{\mathcal{P}}1.2$ can be transformed into

$$\begin{aligned}\hat{\mathcal{P}}1.2 : &\max_{\boldsymbol{\theta}_l} \gamma_{b,i}(\boldsymbol{\theta}_l)\\ \text{s.t.} \quad &\mathcal{C}8\end{aligned} \tag{28}$$

One can observe that $\hat{\mathcal{P}}1.2$ is still a non-convex optimization problem and cannot be efficiently solved. Inspired by the traditional majorization-minimization (MM) algorithm, denote $\boldsymbol{U} = \boldsymbol{h}_{s,l}\text{diag}(\boldsymbol{h}_{i,l}) \in \mathbb{R}^{M\times K}$, $\boldsymbol{\Phi} = [\mathrm{e}^{\mathrm{j}\theta_{l,1}}, \mathrm{e}^{\mathrm{j}\theta_{l,2}}, \ldots, \mathrm{e}^{\mathrm{j}\theta_{l,K}}]^{\mathrm{T}}$, and $V = \boldsymbol{\Phi}^{\mathrm{H}}\boldsymbol{\Phi}$. Define Q is a constant value which can be given $Q = \boldsymbol{h}_{s,i}^{\mathrm{H}}\boldsymbol{w}_{s,i}\boldsymbol{w}_{s,i}^{\mathrm{H}}\boldsymbol{h}_{s,i}$. As such, the numerator of the objective function of $\hat{\mathcal{P}}1.2$ can be rewritten as

$$\begin{aligned}
&p_i^{\mathrm{tr}}\|\boldsymbol{w}_i^{\mathrm{H}}(\boldsymbol{h}_{s,i} + \boldsymbol{U}\boldsymbol{\Phi})\|^2\\
&= p_i^{\mathrm{tr}}[(\boldsymbol{h}_{s,i}^{\mathrm{H}} + \boldsymbol{\Phi}^{\mathrm{H}}\boldsymbol{U}^{\mathrm{H}})\boldsymbol{w}_{s,i}][\boldsymbol{w}_{s,i}^{\mathrm{H}}(\boldsymbol{h}_{s,i} + \boldsymbol{U}\boldsymbol{\Phi})]\\
&= p_i^{\mathrm{tr}}(Q + \boldsymbol{h}_{s,i}^{\mathrm{H}}\boldsymbol{w}_{s,i}\boldsymbol{w}_{s,i}^{\mathrm{H}}\boldsymbol{U}\boldsymbol{\Phi}\\
&\quad + \boldsymbol{\Phi}^{\mathrm{H}}\boldsymbol{U}^{\mathrm{H}}\boldsymbol{w}_{s,i}\boldsymbol{w}_{s,i}^{\mathrm{H}}\boldsymbol{h}_{s,i} + \boldsymbol{\Phi}^{\mathrm{H}}\boldsymbol{U}^{\mathrm{H}}\boldsymbol{w}_{s,i}\boldsymbol{w}_{s,i}^{\mathrm{H}}\boldsymbol{U}\boldsymbol{\Phi})\\
&= p_i^{\mathrm{tr}}\Bigg[\boldsymbol{\Phi}^{\mathrm{H}}\left(\frac{Q}{V}\boldsymbol{I}_K + \boldsymbol{U}^{\mathrm{H}}\boldsymbol{w}_{s,i}\boldsymbol{w}_{s,i}^{\mathrm{H}}\boldsymbol{U}\right)\boldsymbol{\Phi}\\
&\quad + 2\mathrm{Re}\{\boldsymbol{\Phi}^{\mathrm{H}}\boldsymbol{U}^{\mathrm{H}}\boldsymbol{w}_{s,i}\boldsymbol{w}_{s,i}^{\mathrm{H}}\boldsymbol{h}_{s,i}\}\Bigg]\\
&\overset{(a)}{=} \boldsymbol{\Phi}^{\mathrm{H}}\boldsymbol{Y}\boldsymbol{\Phi} + 2\mathrm{Re}\{\boldsymbol{\Phi}^{\mathrm{H}}\boldsymbol{X}\}
\end{aligned} \tag{29}$$

where step (a) holds for $\boldsymbol{X} = p_i^{\mathrm{tr}}\boldsymbol{U}^{\mathrm{H}}\boldsymbol{w}_{s,i}\boldsymbol{w}_{s,i}^{\mathrm{H}}\boldsymbol{h}_{s,i} \in \mathbb{R}^{K\times 1}$ and $\boldsymbol{Y} = p_i^{\mathrm{tr}}(\frac{Q}{V}\boldsymbol{I}_K + \boldsymbol{U}^{\mathrm{H}}\boldsymbol{w}_{s,i}\boldsymbol{w}_{s,i}^{\mathrm{H}}\boldsymbol{U}) \in \mathbb{R}^{K\times K}$. Let $\boldsymbol{A} = \sum_{m=1,m\neq i}^{I}\boldsymbol{Y}_m + \frac{\sigma^2}{V}\boldsymbol{I}_K$ and $\boldsymbol{B} = \sum_{m=1,m\neq i}^{I}\boldsymbol{X}_m$. In this way, the denominator of the objective function of $\hat{\mathcal{P}}1.2$ is rewritten as $\sum_{m=1,m\neq i}^{I} p_m^{\mathrm{tr}}\|\boldsymbol{w}_{s,i}^{\mathrm{H}}(\boldsymbol{h}_{s,m} + \boldsymbol{h}_{s,l}\boldsymbol{\Theta}\boldsymbol{h}_{i,l})\|^2 + \sigma^2\|\boldsymbol{w}_{s,i}^{\mathrm{H}}\|^2 = \boldsymbol{\Phi}^{\mathrm{H}}\boldsymbol{A}\boldsymbol{\Phi} + 2\mathrm{Re}\{\boldsymbol{\Phi}^{\mathrm{H}}\boldsymbol{B}\}$. Thus, $\hat{\mathcal{P}}1.2$ can be rewritten as

$$\begin{aligned}\overline{\mathcal{P}}1.2 : &\max_{\boldsymbol{\Phi}} \frac{\boldsymbol{\Phi}^{\mathrm{H}}\boldsymbol{Y}\boldsymbol{\Phi} + 2\mathrm{Re}\{\boldsymbol{\Phi}^{\mathrm{H}}\boldsymbol{X}\}}{\boldsymbol{\Phi}^{\mathrm{H}}\boldsymbol{A}\boldsymbol{\Phi} + 2\mathrm{Re}\{\boldsymbol{\Phi}^{\mathrm{H}}\boldsymbol{B}\}}\\ \text{s.t.} \quad &\mathcal{C}8\end{aligned} \tag{30}$$

Let $\boldsymbol{\Lambda} = \boldsymbol{\Phi}^{\mathrm{H}}\boldsymbol{Y}\boldsymbol{\Phi} + 2\mathrm{Re}\{\boldsymbol{\Phi}^{\mathrm{H}}\boldsymbol{X}\}$ and $\boldsymbol{\Sigma} = \boldsymbol{\Phi}^{\mathrm{H}}\boldsymbol{A}\boldsymbol{\Phi} + 2\mathrm{Re}\{\boldsymbol{\Phi}^{\mathrm{H}}\boldsymbol{B}\}$ as the intermediate variables. And let $\boldsymbol{E} = \frac{\boldsymbol{\Lambda}_0}{\boldsymbol{\Sigma}_0^2}\boldsymbol{A} - \frac{1}{\boldsymbol{\Sigma}_0}\boldsymbol{Y}$ and $\boldsymbol{F} = \frac{\boldsymbol{\Lambda}_0}{\boldsymbol{\Sigma}_0^2}\boldsymbol{B} - \frac{1}{\boldsymbol{\Sigma}_0}\boldsymbol{X}$. Define the function $f(\boldsymbol{\Lambda}, \boldsymbol{\Sigma}) = \frac{\boldsymbol{\Lambda}}{\boldsymbol{\Sigma}}$, where the lower bound of $f(\boldsymbol{\Lambda}, \boldsymbol{\Sigma})$ can be obtained by taking its first-order Taylor expansion, one has

$$\begin{aligned}
f(\boldsymbol{\Lambda}, \boldsymbol{\Sigma}) &\geq f(\boldsymbol{\Lambda}_0, \boldsymbol{\Sigma}_0) + \frac{1}{\boldsymbol{\Sigma}_0}(\boldsymbol{\Lambda} - \boldsymbol{\Lambda}_0) - \frac{\boldsymbol{\Lambda}_0}{\boldsymbol{\Sigma}_0^2}(\boldsymbol{\Sigma} - \boldsymbol{\Sigma}_0)\\
&= f(\boldsymbol{\Lambda}_0, \boldsymbol{\Sigma}_0) + \frac{1}{\boldsymbol{\Sigma}_0}\boldsymbol{\Lambda} - \frac{\boldsymbol{\Lambda}_0}{\boldsymbol{\Sigma}_0^2}\boldsymbol{\Sigma}\\
&= f(\boldsymbol{\Lambda}_0, \boldsymbol{\Sigma}_0) + \boldsymbol{\Phi}^{\mathrm{H}}\left(\frac{1}{\boldsymbol{\Sigma}_0}\boldsymbol{Y} - \frac{\boldsymbol{\Lambda}_0}{\boldsymbol{\Sigma}_0^2}\boldsymbol{A}\right)\boldsymbol{\Phi}\\
&\quad + 2\mathrm{Re}\left\{\boldsymbol{\Phi}^{\mathrm{H}}\left(\frac{1}{\boldsymbol{\Sigma}_0}\boldsymbol{X} - \frac{\boldsymbol{\Lambda}_0}{\boldsymbol{\Sigma}_0^2}\boldsymbol{B}\right)\right\}\\
&= f(\boldsymbol{\Lambda}_0, \boldsymbol{\Sigma}_0) - \boldsymbol{\Phi}^{\mathrm{H}}\boldsymbol{E}\boldsymbol{\Phi} - 2\mathrm{Re}\{\boldsymbol{\Phi}^{\mathrm{H}}\boldsymbol{F}\}
\end{aligned} \tag{31}$$

As such, $\overline{\mathcal{P}}1.2$ can be transformed into

$$\begin{aligned}\dot{\mathcal{P}}1.2 : &\min_{\boldsymbol{\Phi}} \boldsymbol{\Phi}^{\mathrm{H}}\boldsymbol{E}\boldsymbol{\Phi} + 2\mathrm{Re}\{\boldsymbol{\Phi}^{\mathrm{H}}\boldsymbol{F}\}\\ \text{s.t.} \quad &\mathcal{C}8\end{aligned} \tag{32}$$

Define $\lambda_{\max}(\boldsymbol{E})$ as the maximum eigenvalue of $\boldsymbol{E}$. Since $\boldsymbol{\Phi}^{\mathrm{H}}\lambda_{\max}(\boldsymbol{E})\boldsymbol{I}_K\boldsymbol{\Phi} = V\lambda_{\max}(\boldsymbol{E})$, one has

$$\begin{aligned}
&\boldsymbol{\Phi}^{\mathrm{H}}\boldsymbol{E}\boldsymbol{\Phi} + 2\mathrm{Re}\{\boldsymbol{\Phi}^{\mathrm{H}}\boldsymbol{F}\}\\
&\leq \boldsymbol{\Phi}^{\mathrm{H}}\lambda_{\max}(\boldsymbol{E})\boldsymbol{I}_K\boldsymbol{\Phi} + \boldsymbol{\Phi}_0^{\mathrm{H}}(\lambda_{\max}(\boldsymbol{E})\boldsymbol{I}_K - \boldsymbol{E})\boldsymbol{\Phi}_0\\
&\quad - 2\mathrm{Re}\{\boldsymbol{\Phi}^{\mathrm{H}}(\lambda_{\max}(\boldsymbol{E})\boldsymbol{I}_K - \boldsymbol{E})\boldsymbol{\Phi}_0\} + 2\mathrm{Re}\{\boldsymbol{\Phi}^{\mathrm{H}}\boldsymbol{F}\}
\end{aligned} \tag{33}$$

Define $\boldsymbol{\Phi}^g$ as the value of $\boldsymbol{\Phi}$ obtained in the g-th iteration. To this respect, one can utilize $\boldsymbol{\Phi}^g$ to replace $\boldsymbol{\Phi}_0$ by generating a series of feasible vectors. As such, $\dot{\mathcal{P}}1.2$ can be reformulated as

$$\begin{aligned}\ddot{\mathcal{P}}1.2 : &\max_{\boldsymbol{\Phi}} \mathrm{Re}\{\boldsymbol{\Phi}^{\mathrm{H}}[(\lambda_{\max}(\boldsymbol{E})\boldsymbol{I}_K - \boldsymbol{E})\boldsymbol{\Phi}^g - \boldsymbol{F}]\}\\ \text{s.t.} \quad &\mathcal{C}8\end{aligned} \tag{34}$$

According to Proposition 2, the optimal solution to $\ddot{\mathcal{P}}1.2$ can be given as $\boldsymbol{\Phi}^* = \mathrm{e}^{\mathrm{j}\arg\{(\lambda_{\max}(\boldsymbol{E})\boldsymbol{I}_K - \boldsymbol{E})\boldsymbol{\Phi}^g - \boldsymbol{F}\}}$ with the corresponding $\boldsymbol{\theta}_l^* = \arg\{(\lambda_{\max}(\boldsymbol{E})\boldsymbol{I}_K - \boldsymbol{E})\boldsymbol{\Phi}^g - \boldsymbol{F}\}$.

Proposition 2 The optimal solution $\boldsymbol{\Phi}$ to $\ddot{\mathcal{P}}1.2$ can be given as $\boldsymbol{\Phi}^* = \mathrm{e}^{\mathrm{j}\arg\{(\lambda_{\max}(\boldsymbol{E})\boldsymbol{I}_K - \boldsymbol{E})\boldsymbol{\Phi}^g - \boldsymbol{F}\}}$.

Proof Denote $\boldsymbol{G} = [g_1, g_2, \ldots, g_K]^{\mathrm{T}}$. One can obtain that $\boldsymbol{G} = \{[\lambda_{\max}(\boldsymbol{E})\boldsymbol{I}_K - \boldsymbol{E}]\boldsymbol{\Phi}^g - \boldsymbol{F}\} \in \mathbb{R}^{K\times 1}$. Recall that when $a \geq 0$ and $b \geq 0$, the minimal value of $a^2 + b^2$ can be obtained via $2ab \leq a^2 + b^2$ if and only if $a = b$. In this way, one has

$$\begin{aligned}
\mathrm{Re}\{\boldsymbol{\Phi}^{\mathrm{H}}\boldsymbol{G}\} &= g_1\cos\theta_{l,1} + g_2\cos\theta_{l,2} + \cdots + g_K\cos\theta_{l,K}\\
&\leq \frac{1}{2}(g_1^2 + \cos^2\theta_{l,1}) + \frac{1}{2}(g_2^2 + \cos^2\theta_{l,2})\\
&\quad + \cdots + \frac{1}{2}(g_K^2 + \cos^2\theta_{l,K})
\end{aligned} \tag{35}$$

One can observe that the optimal value of $\mathrm{Re}\{\boldsymbol{\Phi}^{\mathrm{H}}\boldsymbol{G}\}$ can be obtained if and only if $g_k = \cos\theta_{l,k}$, $k \in \{1, 2, \ldots, K\}$. As such, the corresponding optimal value of $\theta_{l,k}$ can be given as

$$\theta_{l,k}^* = \arccos(g_k) \tag{36}$$

As a result, the corresponding optimal solution $\boldsymbol{\Phi}$ to $\ddot{\mathcal{P}}1.2$ can be given as $\boldsymbol{\Phi}^* = \mathrm{e}^{\mathrm{j}\arg\{(\lambda_{\max}(\boldsymbol{E})\boldsymbol{I}_K - \boldsymbol{E})\boldsymbol{\Phi}^g - \boldsymbol{F}\}}$.

This completes the proof.

In this paper, to evaluate the fitness values of $\boldsymbol{u}_l^g$ and $\boldsymbol{q}_l^g$, which can measure the solution quality to $\widetilde{\mathcal{P}}1.2$, the fitness function can be defined as

$$f(\boldsymbol{u}_l^g)=\frac{D_i^l}{\log_2(1+\gamma_{b,i}(\boldsymbol{\theta}_l^*,\boldsymbol{u}_l^g))} \tag{37}$$

Selection The selection operator is performed to select the offspring between $\boldsymbol{u}_l^g$ and $\boldsymbol{q}_l^g$ to the next iteration based on their fitness values, which can be expressed as

$$\boldsymbol{q}_l^{g+1}=\begin{cases}\boldsymbol{u}_l^g, & \text{if } f(\boldsymbol{u}_l^g)\le f(\boldsymbol{q}_l^g)\\ \boldsymbol{q}_l^g, & \text{otherwise}\end{cases} \tag{38}$$

Note that the optimized coordinate $\boldsymbol{q}_l^*$ of UAV l and phase shift-vector $\boldsymbol{\theta}_l^*$ of IRS l can be obtained when the enhanced DE algorithm reaches convergence or reaches the maximum number of iterations $g_{\max}$. The framework of the proposed solution is given in Section IV (see Algorithm 1). Note that B_{sum} indicates the sum of uplink and downlink bandwidth. The complexity analysis of the proposed algorithm can be roughly given as $\mathcal{O}(I+Ig_{\max}\log(\frac{1}{\epsilon^{\text{th}}}))$, where ϵ^{th} is the predetermined convergence accuracy parameter.

IV. Numerical Results

In this section, numerous selected significant results are demonstrated to verify the effectiveness of the proposed solution. The significant simulation parameters are given as follows. USVs are assumed to be randomly distributed in an area of 250 m × 250 m. The range of each UAV hovering height H is set to $[30,100]$ m [28]. The maximum flight speed of each UAV is set to 30 m/s. SAT-USV link is assumed as a controllable non-line-of-sight channel when utilizing IRS technique. In this same manner with [29], SAT-UAV link and UAV-USV link are both assumed as LOS channel. The PL exponents of SAT-USV link, SAT-UAV link, and UAV-USV link are set as 3.5, 2.2, and 2.2, respectively. The transmission power of each USV i is set as $p_i^{\text{tr}}=2$ W and the noise power σ^2 is -70 dBm. The task data size D_i^l generated by USV i and remote input data size D_i^s designated from SAT s and output data size are set to $[1,20]\times10^4$ bits. The maximum allowable time to execute U_i is set as 10 s. The computation capability of each USV and edge server are set to 1×10^5 CPU cycles/s and 1×10^7 CPU cycles/s, respectively. The convergence accuracy of the proposed solution is 10^{-5}. Two advanced algorithms, e.g., RandPhase algorithm and MM algorithm, are selected to compare with the proposed solution. The detailed information is summarized in Algorithm 1.

Algorithm 1 The framework of the proposed solution

Input: I, L, K, S, ϵ^{th}, $w_{s,i}$, $h_{s,i}$, $h_{s,l}$, p^{tr}, $g_{\max}$;
Output: $\boldsymbol{\alpha}^*$, $\boldsymbol{c}^*$, $\boldsymbol{x}^*$, $\boldsymbol{q}^*$, $\boldsymbol{\theta}^*$, B_i^U, and B_i^D;
Initialize: $\boldsymbol{q}_0$, $\boldsymbol{\theta}_0$;
Set $g=1$, $\boldsymbol{q}^g=\boldsymbol{q}_o$, $\boldsymbol{\theta}^g=\boldsymbol{\theta}_0$;
Divide $\mathcal{P}1$ into subproblems $\mathcal{P}1.1$ and $\mathcal{P}1.2$;
//The Joint Optimization of $\boldsymbol{\alpha}$, $\boldsymbol{c}$, and $\boldsymbol{x}$
Transform $\mathcal{P}1.1$ into $\hat{\mathcal{P}}1.1$;
Solve $\hat{\mathcal{P}}1.1$, and obtain the optimized $\boldsymbol{\alpha}^*$, $\boldsymbol{c}^*$ and $\boldsymbol{x}^*$;
//The Joint Optimization of $\boldsymbol{q}$ and $\boldsymbol{\theta}$
while $g<=g_{\max}$ or $\epsilon_{\text{DE}}^g>=\epsilon^{\text{th}}$ **do**
  Substitute $\boldsymbol{\alpha}^*$, $\boldsymbol{c}^*$, and $\boldsymbol{x}^*$ into $\mathcal{P}1.2$;
  Transform $\mathcal{P}1.2$ into $\widetilde{\mathcal{P}}1.2$;
  Perform mutation according to (26);
  Perform crossover according to (27);
  Given any feasible $\boldsymbol{q}$, transform $\widetilde{\mathcal{P}}1.2$ into $\hat{\mathcal{P}}1.2$;
  Transform $\hat{\mathcal{P}}1.2$ into $\overline{\mathcal{P}}1.2$ according to (30);
  Transform $\overline{\mathcal{P}}1.2$ into $\dot{\mathcal{P}}1.2$ according to (32);
  Transform $\dot{\mathcal{P}}1.2$ into $\ddot{\mathcal{P}}1.2$ according to (34);
  Solve $\ddot{\mathcal{P}}1.2$ and obtain $\boldsymbol{\theta}^{g+1}$;
  Substitute $\boldsymbol{\theta}^{g+1}$ into (35) and obtain $f(\boldsymbol{q}^g)$ and $f(\boldsymbol{u}^g)$;
  if $f(\boldsymbol{u}^g)<f(\boldsymbol{q}^g)$ **then**
    $\boldsymbol{q}^{g+1}=\boldsymbol{u}^g$;
  else
    $\boldsymbol{q}^{g+1}=\boldsymbol{q}^g$;
  end
  Compute $\epsilon_{\text{DE}}^{g+1}=\frac{B_{\text{sum}}(\boldsymbol{q}^{g+1},\boldsymbol{\theta}^{g+1})-B_{\text{sum}}(\boldsymbol{q}^g,\boldsymbol{\theta}^g)}{B_{\text{sum}}(\boldsymbol{q}^g,\boldsymbol{\theta}^g)}$;
  $g=g+1$;
end
Update $\boldsymbol{\alpha}^*$, $\boldsymbol{c}^*$, $\boldsymbol{x}^*$, $\boldsymbol{q}^*$, $\boldsymbol{\theta}^*$, B_i^U, and B_i^D.

MM algorithm The majorization-minimization algorithm (refer to MM in the following) aims to maximize the SINR by replacing the upper bound minimization step with a lower bound maximization step. The detailed information regarding MM algorithm can be found in [30].

RandPhase algorithm The random phase algorithm (refer to RandPhase in the following) aims to maximize the SINR by randomly generating the phase shift-vector of IRS and the hovering coordinate of each UAV [31]. The joint optimization of USVs offloading decision, caching decision, and task execution mode selection is identical to the proposed solution.

The relationship between the sum of uplink and downlink bandwidth and the number of USVs is shown in Figure 2. One can observe that as the number of USVs increases, the sum of uplink and downlink bandwidth correspondingly increases. Moreover, one can observe that the proposed solution is capable of decreasing the sum of uplink and downlink bandwidth consumption in comparison with the MM algorithm and the RandPhase algorithm. In particular, the proposed solution realizes the lowest bandwidth consumption at nearly 1.7×10^7 Hz and 8.5×10^6 Hz when $I = 10$ and $I = 5$, respectively, followed by the MM algorithm with the corresponding values at around 1.9×10^7 Hz and 9.7×10^6 Hz. The RandPhase algorithm realizes the worst performance, where the required total bandwidth is around 3.3×10^7 Hz and 1.6×10^7 Hz when $I = 10$ and $I = 5$, respectively.

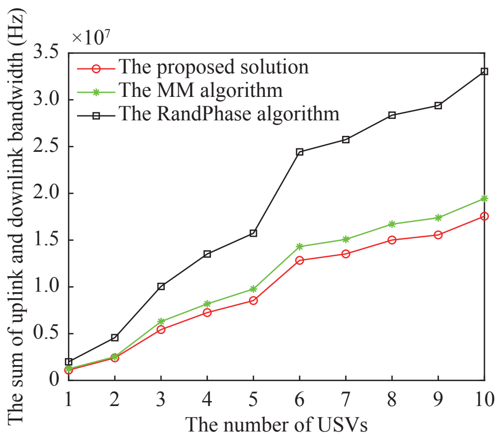

Figure 2 The relationship between the sum of uplink and downlink bandwidth and the number of USVs when $K = 50$ and $H = 30$ m.

Figure 3 demonstrates the sum of uplink and downlink bandwidth versus the number of IRS elements. One can observe that as the number of IRS elements increases, the sum of uplink and downlink bandwidth correspondingly decreases. Moreover, the proposed solution outperforms the MM algorithm and the RandPhase algorithm under the same number of IRS elements. In particular, the proposed solution demands the total bandwidth at nearly 7.4×10^5 Hz and 4.9×10^6 Hz when $K = 150$ and $K = 50$, respectively, followed by the MM algorithm with the corresponding values at around 1.5×10^6 Hz and 5.9×10^6 Hz. The RandPhase algorithm achieves the worst performance; the required total bandwidth is around 2.4×10^6 Hz and 9.6×10^6 Hz when $K = 150$ and $K = 50$, respectively.

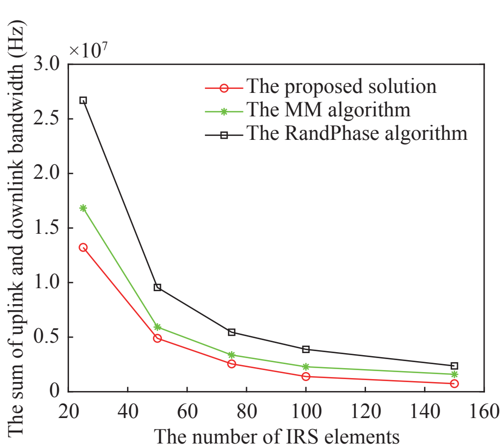

Figure 3 The relationship between the sum of uplink and downlink bandwidth and the number of IRS elements when $I = 10$ and $H = 30$ m.

Figure 4 illustrates the relationship between the sum of uplink and downlink bandwidth and the height of UAVs. One can observe that as the height of UAVs increases, the sum of uplink and downlink bandwidth correspondingly increases. Moreover, the proposed solution realizes the lowest bandwidth consumption in comparison with the RandPhase algorithm and the MM algorithm. In particular, the proposed solution consumes the bandwidth at nearly 4.2×10^7 Hz and 2.3×10^7 Hz when $H = 100$ m and $H = 50$ m, respectively, followed by the MM algorithm with the corresponding values at around 4.7×10^7 Hz and 2.6×10^7 Hz. The RandPhase algorithm realizes the worst performance; the bandwidth is around 5.9×10^7 Hz and 3.3×10^7 Hz when $H = 100$ m and $H = 50$ m, respectively.

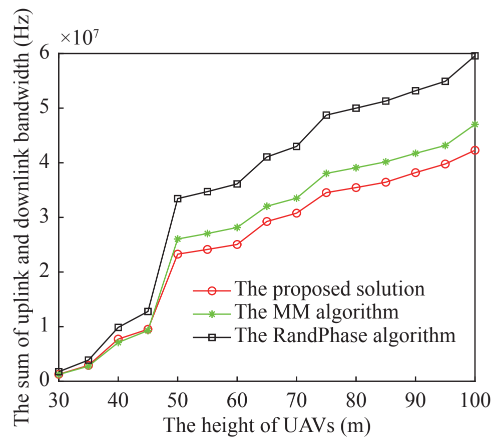

Figure 4 The relationship between the sum of uplink and downlink bandwidth and the height of UAVs when $I = 10$ and $K = 50$.

One can observe that the proposed solution can significantly decrease the required sum of uplink and downlink bandwidth consumption and bring several technical advantages in comparison with two selected advanced algorithms. First, the proposed solution promises each UAV can adaptively adjust IRS phase shift-vector when serving each USV, which can decrease UAVs flying distance and flying time cost compared with the RandPhase algorithm as mentioned in [32]. In addition, the proposed solution is capable of jointly optimizing UAVs trajectory and IRS phase shift-vector, which results in less bandwidth consumption in comparison with the MM algorithm under the same number of IRS elements. One should note that very few thorough studies are focusing on network bandwidth optimization for the proposed novel IRS-assisted hybrid UAV-terrestrial network considering bidirectional data computation, which can be selected for further network performance enhancement research [33].

V. Conclusion

In this paper, a novel IRS-assisted hybrid UAV-terrestrial network architecture of wireless inland waterway communications considering bidirectional tasks is proposed. The sum of the uplink and downlink bandwidth minimization problem is formulated by jointly considering link quality, task execution mode selection, UAVs trajectory, and task execution latency constraints. To solve the formulated challenging problem, we first decouple the original problem into two subproblems. Then, a heuristic algorithm is proposed, where the KKT conditions are utilized to solve the joint optimization problem of USVs offloading decision, caching decision, and task execution mode selection and the enhanced DE algorithm is proposed to solve the joint optimization problem of UAVs trajectory and IRS phase shift-vector design. Numerical results show that the proposed solution can significantly decrease the sum of uplink and downlink bandwidth consumption in comparison with the RandPhase algorithm and MM algorithm. The results also illustrate that the sum of uplink and downlink bandwidth consumption can be remarkably decreased by utilizing the higher number of IRS elements.

Acknowledgements

This work was supported in part by the Natural Science Foundation of China (Grant No. 52201417), the National Key R&D Program of China (Grant No. 2021ZD 0114600), and the Shenzhen Science and Technology Program (Grant No. JCYJ20220818102002005).

References

[1] M. M. Azari, S. Solanki, S. Chatzinotas, *et al.*, "Evolution of non-terrestrial networks from 5G to 6G: A Survey," *IEEE Communications Surveys & Tutorials*, vol. 24, no. 4, pp. 2633–2672, 2022.

[2] M. Vaezi, A. Azri, S. R. Khosravirad, *et al.*, "Cellular, wide-area, and non-terrestrial IoT: A survey on 5G advances and the road toward 6G," *IEEE Communications Surveys & Tutorials*, vol. 24, no. 2, pp. 1117–1174, 2022.

[3] B. Qian, H. B. Zhou, T. Ma, *et al.*, "Multi-operator spectrum sharing for massive IoT coexisting in 5G/B5G wireless networks," *IEEE Journal on Selected Areas in Communications*, vol. 39, no. 3, pp. 881–895, 2021.

[4] T. Taleb, K. Samdanis, B. Mada, *et al.*, "On multi-access edge computing: A survey of the emerging 5G network edge cloud architecture and orchestration," *IEEE Communications Surveys & Tutorials*, vol. 19, no. 3, pp. 1657–1681, 2017.

[5] A. Dallolio, G. Quintana-Diaz, E. Honoré-Livermore, *et al.*, "A satellite-USV system for persistent observation of mesoscale oceanographic phenomena," *Remote Sensing*, vol. 13, no. 16, article no. 3229, 2021.

[6] Q. Q. Wu, S. W. Zhang, B. X. Zheng, *et al.*, "Intelligent reflecting surface-aided wireless communications: A tutorial," *IEEE Transactions on Communications*, vol. 69, no. 5, pp. 3313–3351, 2021.

[7] Q. S. Ai, X. H. Qiao, Y. Z. Liao, *et al.*, "Joint optimization of USVs communication and computation resource in IRS-aided wireless inland ship MEC networks," *IEEE Transactions on Green Communications and Networking*, vol. 6, no. 2, pp. 1023–1036, 2022.

[8] Q. Q. Wu and R. Zhang, "Towards smart and reconfigurable environment: Intelligent reflecting surface aided wireless network," *IEEE Communications Magazine*, vol. 58, no. 1, pp. 106–112, 2020.

[9] S. Basharat, S. A. Hassan, H. Pervaiz, *et al.*, "Reconfigurable intelligent surfaces: Potentials, applications, and challenges for 6G wireless networks," *IEEE Wireless Communications*, vol. 28, no. 6, pp. 184–191, 2021.

[10] X. W. Pang, M. Sheng, N. Zhao, *et al.*, "When UAV meets IRS: Expanding air-ground networks via passive reflection," *IEEE Wireless Communications*, vol. 28, no. 5, pp. 164–170, 2021.

[11] Y. Liao, J. Liu, X. Chen, Y. Han, Q. Ai, and G. M. Muntean, "Energy minimization of inland waterway USVs for IRS-assisted hybrid UAV-terrestrial MEC network," *IEEE Transactions on Vehicular Technology*, 2023.

[12] A. Alkhatieb, K. Rabie, X. W. Li, *et al.*, "IRS-aided UAV for future wireless communications: A survey and research opportunities," *arXiv preprint*, arXiv: 2212.06015, 2022.

[13] S. M. A. Huda and S. Moh, "Survey on computation offloading in UAV-Enabled mobile edge computing," *Journal of Network and Computer Applications*, vol. 201, article no. 103341, 2022.

[14] M. Abrar, U. Ajmal, Z. M. Almohaimeed, *et al.*, "Energy efficient UAV-enabled mobile edge computing for IoT devices: A review," *IEEE Access*, vol. 9, pp. 127779–127798, 2021.

[15] G. F. Pan, J. Ye, J. P. An, *et al.*, "When full-duplex transmission meets intelligent reflecting surface: Opportunities and challenges," *arXiv preprint*, arXiv: 2005.12561, 2020.

[16] S. Malik, P. Saxena, and Y. H. Chung, "Performance analysis of a UAV-based IRS-assisted Hybrid RF/FSO link with pointing and phase shift Errors," *Journal of Optical Communications and Networking*, vol. 14, no. 4, pp. 303–315, 2022.

[17] Q. Liu, S. L. Sun, B. Rong, *et al.*, "Intelligent reflective surface based 6G communications for sustainable energy infrastructure," *IEEE Wireless Communications*, vol. 28, no. 6, pp. 49–55, 2021.

[18] J. R. Xu, X. Kang, R. H. X. Zhang, *et al.*, "Joint power and trajectory optimization for IRS-aided master-auxiliary-UAV-powered IoT networks," in *2021 IEEE Global Communications Conference*, Madrid, Spain, pp. 1–6, 2021.

[19] G. J. Chen, Q. Q. Wu, R. Q. Liu, *et al.*, "IRS aided MEC systems with binary offloading: A unified framework for dynamic IRS beamforming," *IEEE Journal on Selected Areas in Communications*, vol. 41, no. 2, pp. 349–365, 2023.

[20] C. W. Wang, X. F. Yu, L. X. Xu, *et al.*, "Multimodal semantic communication accelerated bidirectional caching for 6G MEC," *Future Generation Computer Systems*, vol. 140, pp. 225–237, 2023.

[21] L. T. Y. Zhang, Y. P. Sun, Z. Y. Chen, *et al.*, "Communications-caching-computing resource allocation for bidirectional data computation in mobile edge networks," *IEEE Transactions on Communications*, vol. 69, no. 3, pp. 1496–1509, 2021.

[22] X. F. Chen, C. L. M. G. Wu, T. Chen, *et al.*, "Age of information aware radio resource management in vehicular networks: a proactive deep reinforcement learning perspective," *IEEE Transactions on Wireless Communications*, vol. 19, no. 4, pp. 2268–2281, 2020.

[23] Y. P. Sun, L. T. Y. Zhang, Z. Y. Chen, *et al.*, "Communications-caching-computing tradeoff analysis for bidirectional data computation in mobile edge networks," in *2020 IEEE 92nd Vehicular Technology Conference (VTC2020-Fall)*, Victoria, BC, Canada, pp. 1–5, 2020.

[24] Y. P. Sun, Z. Y. Chen, M. X. Tao, *et al.*, "Bandwidth gain from mobile edge computing and caching in wireless multicast systems," *IEEE Transactions on Wireless Communications*, vol. 19, no. 6, pp. 3992–4007, 2020.

[25] Y. Cheng, Y. Z. Liao, and X. J. Zhai, "Energy-efficient resource allocation for UAV-empowered mobile edge computing system," in *IEEE/ACM 13th International Conference on Utility and Cloud Computing*, Leicester, UK, pp. 408–413, 2020.

[26] B. Ghojogh, A. Ghodsi, F. Karray, *et al.*, "KKT conditions, first-order and second-order optimization, and distributed optimization: tutorial and survey," *arXiv preprint*, arXiv: 2110.01858, 2021.

[27] P. Q. Huang, Y. Wang, K. Z. Wang, *et al.*, "Differential evolution with a variable population size for deployment optimization in a UAV-Assisted IoT data collection system," *IEEE Transactions on Emerging Topics in Computational Intelligence*, vol. 4, no. 3, pp. 324–335, 2020.

[28] M. Fu, Y. Zhou, Y. M. Shi, *et al.*, "UAV aided over-the-air computation," *IEEE Transactions on Wireless Communica-*

tions, vol. 21, no. 7, pp. 4909–4924, 2022.

[29] D. Ma, M. Ding, and M. Hassan, “Enhancing cellular communications for UAVs via intelligent reflective surface,” in *IEEE Wireless Communications and Networking Conference (WCNC)*, Seoul, Korea, pp. 1–6, 2020.

[30] Y. Sun, P. Babu, and D. P. Palomar, “Majorization-minimization algorithms in signal processing, communications, and machine learning,” *IEEE Transactions on Signal Processing*, vol. 65, no. 3, pp. 794–816, 2017.

[31] Y. Z. Liao, J. Y. Liu, Y. Han, *et al.*, “Energy minimization for IRS-assisted UAV-empowered wireless communications,” in *International Conference on Mobility, Sensing and Networking*, Guangzhou, China, pp. 1001–1006, 2022.

[32] E. Björnson, Ö. Özdogan, and E. G. Larsson, “Intelligent reflecting surface versus decode-and-forward: How large surfaces are needed to beat relaying,” *IEEE Wireless Communications Letters*, vol. 9, no. 2, pp. 244–248, 2020.

[33] C. S. You, Z. Y. Kang, Y. Zeng, *et al.*, “Enabling smart reflection in integrated air-ground wireless network: IRS Meets UAV,” *IEEE Wireless Communications*, vol. 28, no. 6, pp. 138–144, 2021.

Yangzhe LIAO received the B.S. degree in measurement and control technology from Northeastern University, Shenyang, China, in 2013 and the Ph.D. degree from The University of Warwick, Coventry, UK, in 2017. Dr. Liao is an Associate Professor at the School of Information Engineering, Wuhan University of Technology, Wuhan, China. His research interests include mobile edge computing and mobile computing.
(Email: yangzhe.liao@whut.edu.cn)

Lin LIU is currently pursuing the M.S. degree in information and communication engineering with the School of Information Engineering, Wuhan University of Technology, Wuhan, China. Her research interests mainly focus on wireless resource allocation and network optimization.
(Email: wutliulin@whut.edu.cn)

Yuanyan SONG is currently pursuing the M.S. degree in electronic information with the School of Information Engineering, Wuhan University of Technology, Wuhan, China. His research interests include mobile edge computing and resource allocation in wireless communications.
(Email: 288405@whut.edu.cn)

Ning XU received the Ph.D. degree in electronic science and technology from University of Electronic Science and Technology of China, Chengdu, China, in 2003, and was a Postdoctoral Fellow with Tsinghua University, Beijing, China, from 2003 to 2005. Prof. Xu is a Professor at the School of Information Engineering, Wuhan University of Technology, Wuhan, China. His research interests include computer-aided design of VLSI circuits and systems, big data analysis, and artificial intelligence.
(Email: xuning@whut.edu.cn)